

## Upconversion Nanoparticles

International Edition: DOI: 10.1002/anie.201904208  
German Edition: DOI: 10.1002/ange.201904208

## Visualization of Intra-neuronal Motor Protein Transport through Upconversion Microscopy

Xiao Zeng<sup>+</sup>, Shuo Chen<sup>+</sup>, Adam Weitemier, Sanyang Han, Agata Blasiak, Ankshita Prasad, Kezhi Zheng, Zhigao Yi, Baiwen Luo, In-Hong Yang, Nitish Thakor, Chou Chai, Kah-Leong Lim, Thomas J. McHugh,<sup>\*</sup> Angelo H. All,<sup>\*</sup> and Xiaogang Liu<sup>\*</sup>

**Abstract:** Cargo transport along axons, a physiological process mediated by motor proteins, is essential for neuronal function and survival. A current limitation in the study of axonal transport is the lack of a robust imaging technique with a high spatiotemporal resolution to visualize and quantify the movement of motor proteins in real-time and in different depth planes. Herein, we present a dynamic imaging technique that fully exploits the characteristics of upconversion nanoparticles. This technique can be used as a microscopic probe for the quantitative *in situ* tracking of retrograde transport neurons with single-particle resolution in multilayered cultures. This study may provide a powerful tool to reveal dynamic neuronal activity and intra-axonal transport function as well as any associated neurodegenerative diseases resulting from mutation or impairment in the axonal transport machinery.

## Introduction

Dynein-driven retrograde axonal transport delivers intracellular cargoes from the axonal terminal toward the soma.<sup>[1]</sup> This dynamic process regulates many physiological functions in neurons, including nutrient supply, molecular signaling, and the mobility of organelles. Impairment in the neuronal retrograde transport is often associated with neurodegenerative diseases such as Rett syndrome.<sup>[2]</sup> Therefore, early identification and direct visualization of such deficits could provide vital information in screening, diagnosis, and prognosis of axonal transport-related diseases. The direct visual-

ization of a sub-cellular process involving protein molecules or organelles hinges on the nanoscale probes and their luminescent properties. Conventionally, fluorophores like organic dyes,<sup>[3]</sup> fluorescent proteins,<sup>[4]</sup> and quantum dots<sup>[5]</sup> were used for tracking dynein movement. However, these probes have significant limitations, including poor photostability (photo-blinking and photo-bleaching), high autofluorescence, limited imaging depth, and the need for expensive and sophisticated microscopy setups.

Lanthanide-doped upconversion nanoparticles (UCNPs) are one of the few materials that support photon upconversion under continuous-wave laser excitation.<sup>[6]</sup> UCNPs are ideal for use as bioimaging probes because of their multicolor emission tunability,<sup>[7]</sup> excellent photostability,<sup>[8]</sup> and deep-tissue imaging potential.<sup>[9]</sup> In addition, by exciting UCNPs with near-infrared (NIR) light, imaging can be performed without autofluorescence interference. Although luminescence imaging using single UCNPs has been achieved recently with laser scanning microscopy,<sup>[8a,10]</sup> this approach often requires high laser power and focus, which may lead to overheating of biological tissues and a slow image refreshing rate. To image moving objects at a single-particle level, a wide-field illumination is desired. Herein, we demonstrated that single upconversion nanoparticles can be visualized under wide-field NIR illumination at an imaging refresh rate of 7 Hz, which enables zero-autofluorescence imaging and continuous tracking of dynein movement inside multi-layer neuron cultures without signal disruption.



[\*] Dr. X. Zeng,<sup>[†]</sup> Dr. S. Han, Dr. K. Zheng, Z. Yi, Prof. X. Liu  
Department of Chemistry, National University of Singapore  
Singapore 117543 (Singapore)  
E-mail: chmlx@nus.edu.sg

Dr. S. Chen,<sup>[†]</sup> Dr. A. Weitemier, Prof. T. J. McHugh  
Laboratory for Circuit and Behavioral Physiology  
RIKEN Center for Brain Science  
Wakoshi, Saitama 351-0198 (Japan)  
E-mail: tjmcHugh@brain.riken.jp

Dr. A. Blasiak, Dr. A. Prasad, Dr. B. Luo, Prof. I. Yang, Prof. N. Thakor,  
Prof. A. H. All, Prof. X. Liu  
Singapore Institute of Neurotechnology  
National University of Singapore  
Singapore 117456 (Singapore)  
Prof. N. Thakor, Prof. A. H. All  
Department of Biomedical Engineering  
Johns Hopkins School of Medicine  
Baltimore, MD 21205 (USA)  
E-mail: hmn@jhu.edu

Dr. C. Chai, Prof. K. Lim  
Research Department, National Neuroscience Institute  
Singapore 308433 (Singapore)  
and  
Department of Physiology, National University of Singapore  
Singapore 117593 (Singapore)  
Prof. T. J. McHugh  
Department of Life Sciences, Graduate School of Arts and Sciences,  
University of Tokyo  
Tokyo (Japan)  
Prof. A. H. All  
Department of Neurology, Johns Hopkins School of Medicine  
Baltimore, MD 21205 (USA)

[†] These authors contributed equally to this work.

 Supporting information, including experimental details, and the  
 ORCID identification number(s) for the author(s) of this article can  
be found under:  
<https://doi.org/10.1002/anie.201904208>.

## Results and Discussion

We performed luminescence microscopy to validate that UCNPs can be visualized at the single-particle level under a mild excitation power density. Silica-coated NaLuF<sub>4</sub>:Yb<sup>3+</sup>/Er<sup>3+</sup> UCNPs (980 nm excitation; 528, 539, and 650 nm emission) with an average diameter of 60 nm were diluted and spread onto a glass substrate (Figure 1 a–c). By exciting the region of interest with a NIR laser, we observed high-contrast luminescence spots, which were confirmed to be single-particle emissions by scanning electron microscopy (SEM) (Figure 1 d,e). Notably, in the current imaging setup, the NIR laser was illuminated at a wide-field diameter of 150  $\mu$ m, enabling tracking of the movement of each nanoparticle individually and continuously at a fast rate. Widening to a large field of laser illumination significantly lowered the power density to 1 kW cm<sup>-2</sup> and eliminated the risk of overheating. This was confirmed by upconversion thermometry analysis of the samples under study, which reveals a stable temperature of 37 °C after 10 min of continuous 980 nm laser irradiation at 1 kW cm<sup>-2</sup> (Figure S1, Supporting Information).

We investigated the application of UCNPs as a more effective and accurate tool for the visualization of axonal retrograde transport using dorsal root ganglion (DRG)

neurons cultured in a multi-compartment microchamber.<sup>[11]</sup> The microchamber consists of two compartments, one isolating cell somas and the other isolating the axons, interlinked with elongated channels (500  $\mu$ m in length, 10  $\mu$ m in width and height) (Figure 1 f). DRG neurons from rodent embryos were collected and cultured in the soma compartment. After 10 days, axons elongated naturally and passed through the interlinked micro-channels to enter the axonal compartment (Figure 1 g). To ensure that only neuronal axon crosses through the micro-chamber, a glial cell inhibitor, fluorodeoxyuridine (FuDR), was added to the medium, and neuronal identity was confirmed by Neurofilament 200 staining ( $n=3$ , 93.6  $\pm$  1 % of the cells stained positive). Then, on the same day (day 10), UCNPs were added into the axonal compartment, and we observed rapid uptake and transport to the soma compartment as quickly as 3 h after co-culture. It is believed that such transportation of nanoparticles started with their cell uptake through the endocytosis pathway. After entering the cell, upconversion nanoparticles were trapped inside endosomes. Once the membrane receptor on the endosomes binds with cytoplasmic dyneins through protein–protein interactions, the dyneins would carry the nanoparticle-containing endosome and move toward the soma along the microtubule tracks in the axons. Although there are no direct interactions between the upconversion nanoparticles

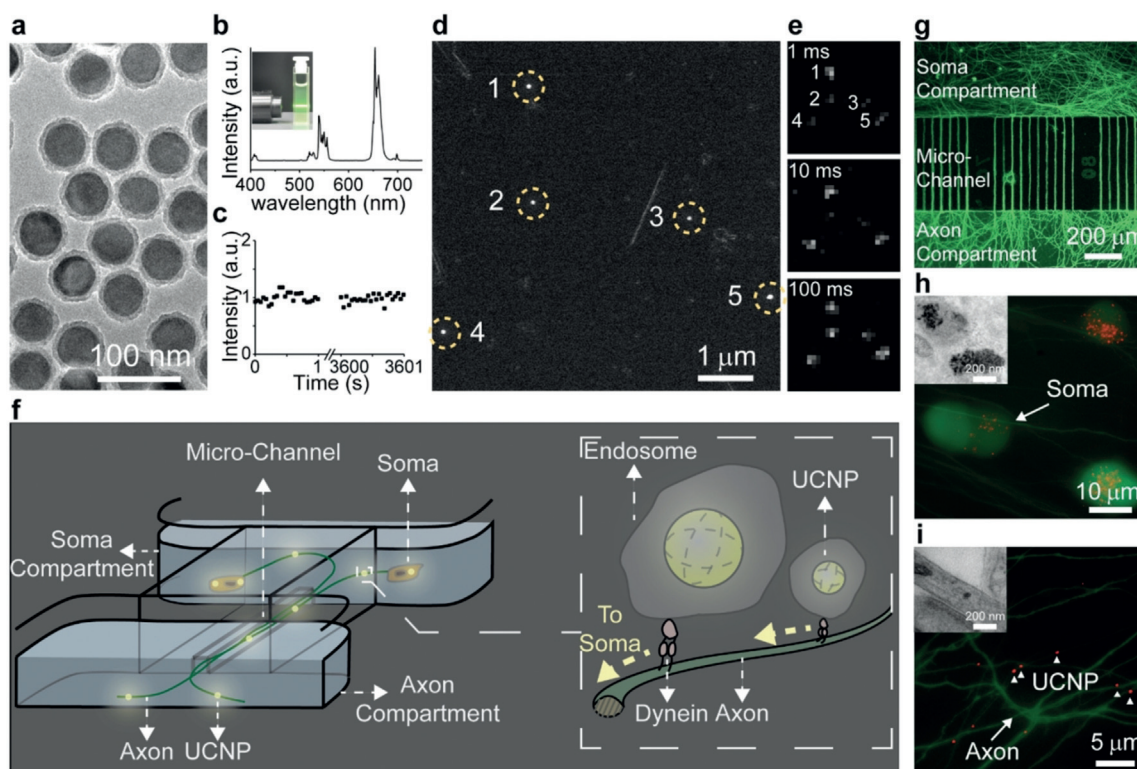


**Figure 1.** a) TEM image of the silica-coated UCNPs. b) Luminescence spectrum of an aqueous solution of the NPs under 980 nm excitation. Inset: Photograph of the solution upon laser excitation. c) The high photostability of the UCNPs under continuous laser excitation. d) SEM image of five UCNPs deposited on a glass substrate. e) Upconversion luminescence microscopy of the same NPs observed in (d). f) Schematic of our two-compartment microchamber connected by microchannels. g) Fluorescence microscopy image of calcein-labeled DRG neurons cultured in the chamber. h) Fluorescence imaging showing the accumulation of UCNPs (red dots) in the soma (green channel) 3 h after their incubation. Inset: Electron microscopy image of UCNPs inside the soma. i) Fluorescence and electron microscopy image (inset) showing the capture of UCNPs inside the axons.

with dyneins, the emission signal from the upconversion nanoparticles can be utilized to report the whereabouts of the cytoplasmic dyneins in real-time.

Real-time luminescence microscopy was conducted to track intra-axonal retrograde transport. Figure S2 in the Supporting Information shows the detection of upconversion luminescence in the soma compartment 3 h after placing UCNPs in the axonal compartment. To visualize the axonal tracts and quantify cell viability, neurons were stained with Calcein AM dye. This staining revealed that even after prolonged (24 h) exposure of axons to UCNPs,  $78.1 \pm 3\%$  of the DRGs remained Calcein AM-positive and showed no propidium iodide signal. We also observed that upconversion luminescence overlaid precisely with the Calcein-stained soma and axonal tracts (Figure 1h,i). This indicates that UCNPs were actively transported by motor proteins along the axonal tracts, rather than by passive nanoparticle diffusion that is prevented by the hydrostatic pressure bias set across the compartment. Transmission electron microscopy (TEM) verified the uptake of UCNPs by axons and their accumulation in the soma (Figure 1h,i; Figure S3 in the Supporting Information). Similar results were obtained with UCNPs coated with functional moieties of both positive and negative charges (Figure S4, Supporting Information). From a technical

point of view, it is noteworthy that UCNPs must disperse well in the culture media to ensure for efficient uptake into the axons and their consequent intra-axonal retrograde transport. Interestingly, we also found that aggregation in poly(acrylic acid)-coated UCNPs (mean diameter  $> 1 \mu\text{m}$ ) leads to failure of intra-axonal transport (Figure S4, Supporting Information).

To visualize the intra-neuronal transport of UCNPs in real time, we recorded video of the upconversion emission in the soma compartment at 7 Hz. In a typical video clip (Figure 2a,b; Video 1 in the Supporting Information), the majority of UCNPs could be seen moving toward the soma along their axonal tracks at an average speed of  $1.71 \pm 0.6 \mu\text{m s}^{-1}$ . They exhibited a “stop and go” movement pattern with occasionally short distance trails of backward movement. Since the non-membrane-bound proteins exhibit slower axonal movement, their “stop and go” movement pattern is considered to be related to intra-axonal cargos that often have relatively long pauses. This pattern is also consistent with the intracellular trajectory of dynein motor proteins.<sup>[12]</sup> The non-photobleaching nature of UCNPs and the large field of view allowed us to track the particle movement along a distance of  $100 \mu\text{m}$  over 5 min without signal attenuation. Meanwhile, the non-photoblinking feature of UCNPs enabled us to contin-

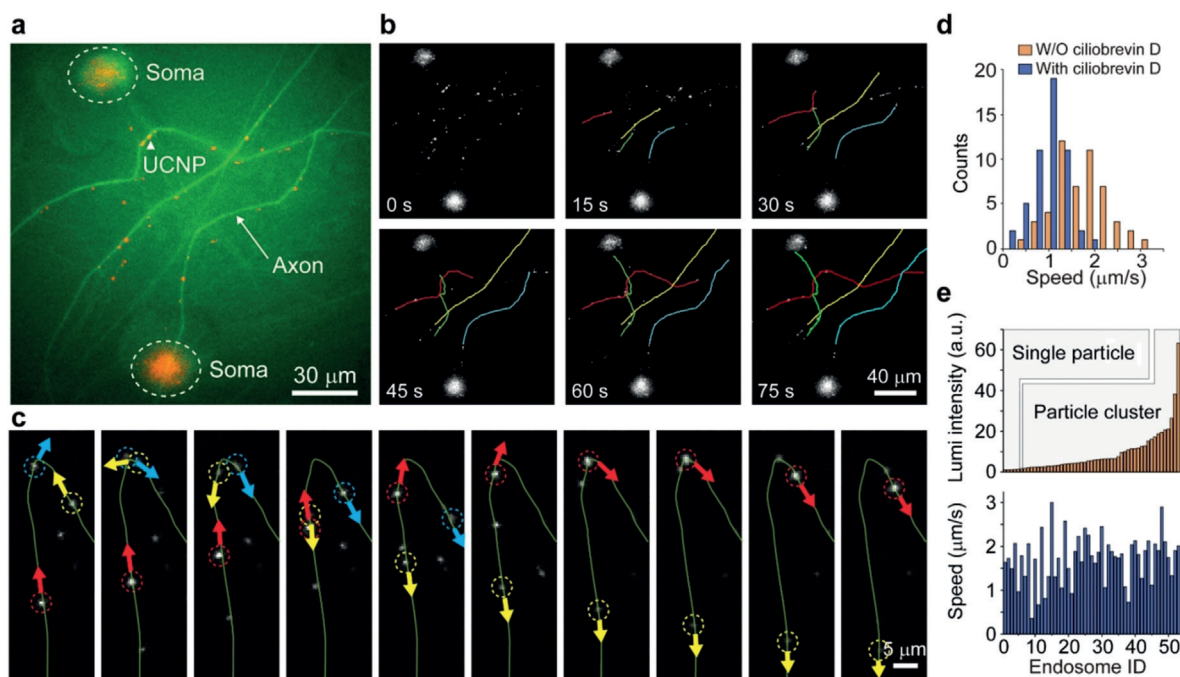


**Figure 2.** a) Luminescence microscopy image showing one frame from a typical dynein-tracking video. The green fluorescence signal originates from calcein-labeled soma and axons (488 nm excitation, 530 nm emission). The red dots are visible emissions arising from the particles' emission (980 nm excitation). b) Tracking of four individual upconversion luminescence spots over a long distance ( $> 100 \mu\text{m}$ ). The trajectories left by the four emission spots match with the shape of the axons shown in (a), indicating that the nanoparticles are traveling along the axon track. In this 100 s video, the movement of 180 UCNPs from the four axons can be analyzed in parallel. c) Tracking of UCNPs traveling in two directions along an axonal (marked in green) taken at 2.2-s time intervals. The retrograde transport is marked by red and blue arrows, while yellow arrows mark the anterograde transport. d) Histogram of dynein's average speed recorded in the presence or absence of dynein inhibitor, ciliobrevin D. e) Luminescence quantification of the number of UCNPs carried by one endosome. The top graph plots the luminous intensity collected from randomly chosen endosomes. The endosome identities are arranged according to the emission intensity of their cargo. Based on emission intensity analysis, the portion of endosomes that contain one UCNPs is highlighted in the graph. Note that a single endosome could carry approximately 60 UCNPs in its lumen. The bottom graph plots the movement speed for each of the endosomes shown in the upper graph, suggesting that dynein movement speed is not affected by the number of UCNPs being carried.



uously track particles at a resolution of 400 nm (Figure S5, Supporting Information). To verify the role of dynein motor protein in intra-axonal UCNPs retrograde transport, a dynein specific inhibitor, ciliobrevin D,<sup>[13]</sup> was added to the neuron culture. Adding 30  $\mu\text{M}$  of ciliobrevin D significantly reduced the intra-axonal transport velocity to  $1.01 \pm 0.4 \mu\text{m s}^{-1}$  from  $1.71 \pm 0.6 \mu\text{m s}^{-1}$  ( $n = 50$  tracking each, two-tailed unpaired *t*-test,  $***p = 1.40 \times 10^{-11}$ ; Figure 2d and Figure S6 in the Supporting Information). This significant reduction in the speed of movement indicates that retrograde transport of UCNPs inside axons is correlated with the dynein function. Meanwhile, we also observed a small percentage of UCNPs (1.6%) constantly moving against the mainstream particle migration direction, which could be attributed to kinesin-driven movement of the particles (Figure 2c). This observation supports the notion that different types of motor proteins function synergistically in regulating the cargo transport inside axons.<sup>[14]</sup>

By analyzing the intensity of upconversion light emission from each of the motor proteins and comparing it to single UCNPs emission intensity, we established that at  $2 \text{ mg mL}^{-1}$  UCNPs concentration, only  $12 \pm 6\%$  of the endosomes contained one UCNPs and the majority of the UCNPs were transported as clusters (up to 60) inside each endosome (Figure 2e). This was also verified and confirmed by the TEM results. Interestingly, we also observed that the speed of dynein movement was not correlated with their cargo mass. Regardless of the size and weight of UCNPs, the visualization of their retrograde transport can be used as an indicator of the cytoplasmic dynein speed of movement.

To demonstrate the feasibility of using the UCNPs-probe as a potential tool for early screening of neurodegenerative diseases, we investigated its application in a cellular model of Rett syndrome (RTT), a disease linked to deficits in intra-axonal cargo transport.<sup>[15]</sup> Clinical diagnosis of RTT relies on identifying the molecular mutation of the MECP2 gene (though not present in all cases) or clinical signs and symptoms, including slow head growth after birth. Therefore, a more sensitive screen that can be applied after early symptoms are detected would empower physicians with improved diagnosis capability, more effective therapeutic interventions, and consequently better clinical outcome.

To study the dynein movement in human neurons, we used a well-established induced pluripotent stem cells (iPSCs) reprogramming technique to convert human fibroblast derived from a patient diagnosed with RTT to cortical neurons (Figure 3a and Figures S7 and S8 in the Supporting Information).<sup>[16]</sup> Then, we cultured iPSC-derived RTT cortical neurons in a two-compartment microchamber that separates soma in the soma compartment from axons in the axonal compartment.

Since a higher neural stem cells plating density is required to facilitate efficient differentiation and optimal axonal growth across microchannels, the result creates a relatively thick (approximately 30  $\mu\text{m}$ ) 3D cellular culture (Figure 3b). Such thickness is a limitation for conventional imaging probes such as total internal reflection fluorescence (TIRF) microscopy, which has an imaging depth of less than 400 nm. UCNPs-based microscopy overcomes the challenge of imaging depth

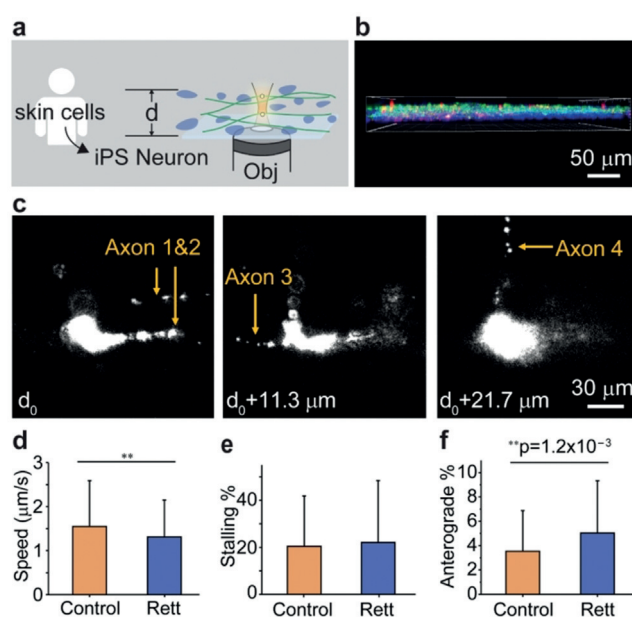


**Figure 3.** a) The schematic process of converting fibroblasts to neurons through iPSC reprogramming. Multi-layered, high-density neurons were cultured in the chamber to ensure their survival rate. b) Side-view confocal microscopy image of the multi-layered neuron cultures. The blue and green channels refer to nucleus and axons, respectively. c) Upconversion luminescence images of dynein, viewed at different z-depths. The three images were collected at the same x-axis and y-axis location. By changing the focal point of the lens, four axons in three different imaging planes could be detected. d) Dynein's speed collected from both healthy neurons and Rett syndrome patient neurons. e) The probability of dynein stalling in healthy neurons and Rett syndrome patient neurons. f) The probability of dynein anterograde movement in both healthy neurons and Rett syndrome patient neurons.

without any compromise in image resolution and quality. Using upconversion microscopy, we showed that the intra-axonal movement of UCNPs could be easily identified and tracked over a long period at different focal z-planes (Figure 3c and Video 2 in the Supporting Information). We further investigated the impairment of retrograde axonal transport in cortical neurons derived from iPSCs of patients with Rett syndrome and compared them to control iPSC-derived healthy neurons (Figure S9 and Videos 3 and 4 in the Supporting Information). To assess the characteristics of intra-axonal retrograde transport, we described the following three parameters: velocity, stalling ("stop and go") frequency, and backward movement of UCNPs.

The average velocity of UCNPs intra-axonal retrograde transport in control cortical neurons ( $n = 247$  tracings from 82 axons) was calculated at  $1.55 \pm 1.0 \mu\text{m s}^{-1}$ , which was significantly faster than RTT's cortical neurons ( $n = 291$  tracings from 92 axons) at  $1.31 \pm 0.8 \mu\text{m s}^{-1}$  ( $***p = 0.032$ , two-tailed unpaired *t*-test with Welch's correction, 3 independent experiments; Figure 3d). As retrograde transport in human cortical neurons exhibited the "stop and go" characteristics, we also assessed the stalling time and the frequency of backward movement during the transport of UCNPs. Stalling is defined as a displacement of less than 0.1  $\mu\text{m}$  from its previous point

of reference. In the control group of neurons, the average stalling time over a 10 s period was  $2.04 \pm 2.2$  s ( $n=260$  tracings) and in the RTT neurons was  $2.21 \pm 2.6$  s ( $n=321$  tracings), which was found to be a statistically non-significant difference ( $p=0.3919$ , two-tailed unpaired  $t$ -test with Welch's correction, 3 independent experiments; Figure 3 e).

The backward movement tendency during the retrograde tracking is defined as directional changes of  $175.01^\circ$  to  $184.99^\circ$  from its previous original point (the first event). Our results indicate that dyneins in RTT cortical neurons spent  $5.03 \pm 4.3\%$  of their entire traveling time in backward movement ( $n=296$  tracings), which is significantly higher than the  $3.54 \pm 3.4\%$  ( $n=260$  tracings) spent in backward movement recorded for the control group (Figure 3 f). The abovementioned three-parameter comparison suggests that our photo-stable UCNP probes allow for reliable and highly sensitive detection of subtle changes in the neuronal retrograde transport.

We demonstrated that UCNPs could be transported from axonal terminals to soma by a dynein protein transport mechanism. We expanded our investigation to test the possibility of utilizing upconversion microscopy also as a retrograde tracing technique for studying neuronal projections in the brain.<sup>[17]</sup> For this aim, silica-coated UCNPs were stereotactically transplanted in the dentate gyrus region of

a mouse brain. Then 72 h later, the mouse brain was harvested, sectioned, and mounted onto sample slides for microscopic examination. At the injection site, UCNPs were confined mainly to a narrow area of  $200 \times 200 \mu\text{m}^2$  within dentate gyrus (Figure S10a, Supporting Information). Interestingly, we observed that neurons in both the supramammillary nucleus (SuM) and entorhinal cortex (Ent) (both over 3 mm far from the injection site), areas known to project to the dentate gyrus, exhibited the distinct spectrum of upconversion emission. High-magnification imaging clearly showed that the nanoparticles were aggregated in the soma of SuM and Ent neurons (Figure S10b–d, Supporting Information). To validate the fact that UCNPs entered these neurons, located far from the injection site, through the dynein-mediated motor protein transport rather than diffusion, we co-administrated UCNPs with retro-beads, a fluorescence-based commercial tracing probe (Lumafluor Retrobeads, red beads), into dentate gyrus (Figure 4 a,b). Both upconversion and retro-bead signals appeared at SuM and Ent regions (Figure 4 c); this observation is in agreement with the previous findings that SuM and Ent neurons project their axons into dentate gyrus.<sup>[18]</sup> Remarkably, among all the luminescently labeled cells, 66% exhibited precise co-localization of upconversion and retro-bead fluorescent signals, indicating that UCNPs and the retro-beads were delivered by

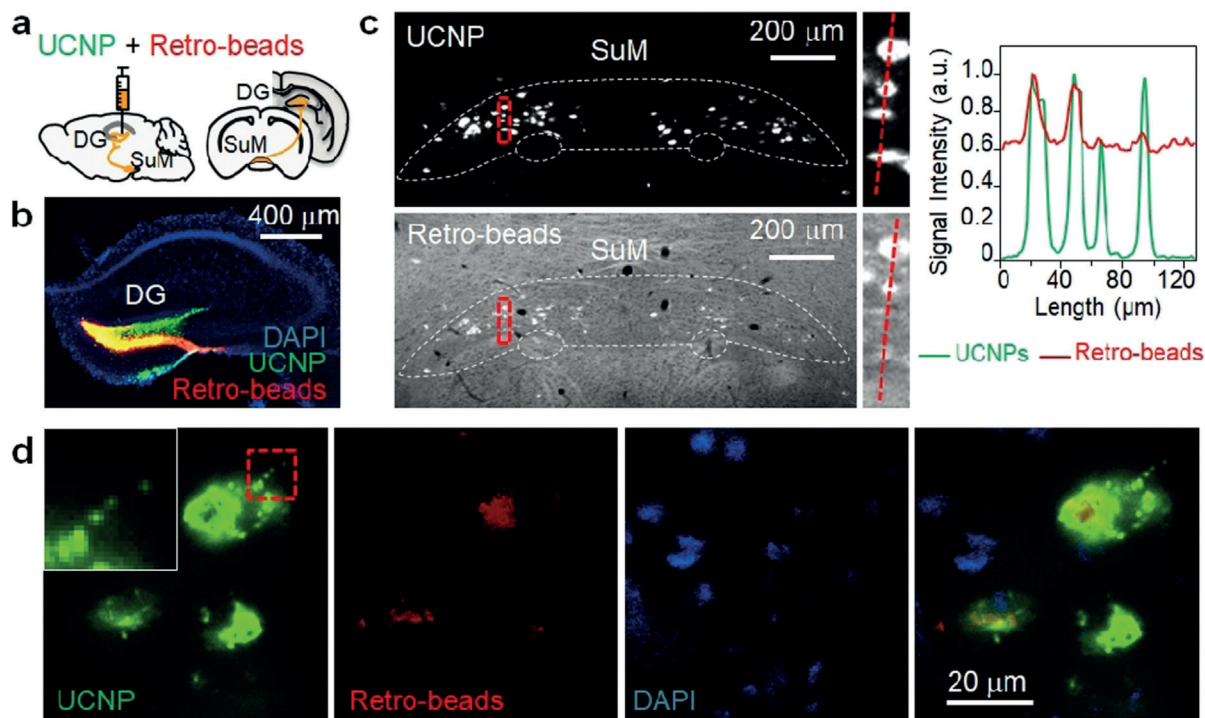


**Figure 4.** a) Schematic concept of retrograde tracing. A mixture of UCNPs and retro-beads was transplanted at the dentate gyrus (DG) in the hippocampus, where dynein motor proteins could subsequently transport them to other regions of the brain. One possible target region was identified as supramammillary nucleus (SuM) in the thalamus, which is 3 mm away from the injection site. b) Luminescence image of the distribution of UCNPs (green) and retro-beads (red) at the DG injection site. Both probes were co-localized at DG with similar diffusion distances. c) Luminescent images of the UCNPs (top) and retro-bead (bottom) distribution at the SuM site. SuM is highlighted by white dashed lines. Four neurons in the red circled region were selected, and their luminescent intensity profile was plotted on the right. UCNPs exhibit a signal-to-noise ratio of 45:1 whereas traditionally used retro-beads yielded a signal-to-noise ratio of 1.3:1. d) High-resolution luminescence images of SuM neurons shown in (c). The first panel, captured in the upconversion channel, shows the emission of UCNPs. The second panel (TRITC channel) shows the emission of retro-beads. The third panel (DAPI channel) shows the location of the nucleus. The last panel shows the merge of panels 1–3, revealing the co-localization of UCNPs and retro-beads.

the same mechanism (Figure 4d). Trails of isolated UCNPs were also found to be localized outside of the soma, which coincided with the dynein-mediated retrograde transport mechanism (Figure 4d, inset). Apart from those dual-labeled cells, 23% of soma exclusively exhibited upconversion luminescence, and 10% of soma exclusively carried retrobead fluorescent signals. These results could be attributed to the different spatial distribution of tracers at the injection site and, even more importantly, to the different imaging contrast for the two types of tracers. It is important to consider that when retrobeads are used, the overwhelming tissue autofluorescence can obscure those weakly labeled cells. In contrast, autofluorescence can be eliminated using the UCNP tracers. The upconversion microscopy also led to high imaging signal-to-noise ratios of up to 45:1 (Figure 4c). Even for tissue samples as thick as 200  $\mu\text{m}$ , retrograde tracing with UCNPs still offered high contrast images (signal-to-noise ratio of 12:1), which revealed the spatial distribution of SuM cells and their projection to dentate gyrus (Figure S11, Supporting Information).

## Conclusions

In conclusion, we demonstrated the use of autofluorescence-free and photo-stable UCNPs for visualization of intra-axonal retrograde transport in real-time. Importantly, this novel technique facilitates the implementation of continuous tracking of UCNP-labeled intra-neuronal motor proteins with an expanded field of view and at different imaging depths. Our experimental data demonstrated that by harnessing the in vitro retrograde transport capability, the upconversion microscopy has potential utility in in vivo settings as a new class of virus-free and high contrast retrograde tracer. This property is fully compatible with conventional fluorescent tracers in performing multi-channel brain circuit mapping as well. The upconversion microscopy could also be considered as a new tool to elucidate the pathophysiological mechanism behind transport dysfunction of intra-neuronal motor proteins and to facilitate early screening of neurodegenerative diseases as well as brain-cell tracing and mapping.

## Acknowledgements

This work was supported by the Singapore Ministry of Education (Grant R143000627112, R143000642112), Singapore National Research Foundation, and the National Natural Science Foundation of China (Grant 21771135, 21701119). We would like to thank S. H. Tan and K. Y. Low from the Electron Microscopy Unit at the National University of Singapore for their technical support in electron microscopy imaging and D. T. B. Loong for his help in acquiring electron microscopy data of neurons and iPSC data.

## Conflict of interest

The authors declare no conflict of interest.

**Keywords:** axon transport · dynein · single-particle resolution · upconversion microscopy · wide-field illumination

**How to cite:** *Angew. Chem. Int. Ed.* **2019**, 58, 9262–9268

*Angew. Chem.* **2019**, 131, 9363–9369

- [1] a) N. Hirokawa, *Science* **1998**, 279, 519–526; b) R. D. Vale, *Cell* **2003**, 112, 467–480; c) A. J. Roberts, T. Kon, P. J. Knight, K. Sutoh, S. A. Burgess, *Nat. Rev. Mol. Cell Biol.* **2013**, 14, 713–726.
- [2] a) E. Chevalier-Larsen, E. L. Holzbaur, *Biochim. Biophys. Acta Mol. Basis Dis.* **2006**, 1762, 1094–1108; b) G. B. Stokin, C. Lillo, T. L. Falzone, R. G. Brusch, E. Rockenstein, S. L. Mount, R. Raman, P. Davies, E. Masliah, D. S. Williams, L. S. Goldstein, *Science* **2005**, 307, 1282–1288.
- [3] a) W. Qiu, N. D. Derr, B. S. Goodman, E. Villa, D. Wu, W. Shih, S. L. Reck-Peterson, *Nat. Struct. Mol. Biol.* **2012**, 19, 193–200; b) M. Hafezparast, R. Klocke, C. Ruhrberg, A. Marquardt, A. Ahmad-Annuar, S. Bowen, G. Lalli, A. S. Witherden, H. Hummerich, S. Nicholson, P. J. Morgan, R. Oozageer, J. V. Priestley, S. Averill, V. R. King, S. Ball, J. Peters, T. Toda, A. Yamamoto, Y. Hiraoka, M. Augustin, D. Korthaus, S. Wattler, P. Wabnitz, C. Dickneite, S. Lampel, F. Boehme, G. Peraus, A. Popp, M. Rudelius, J. Schlegel, H. Fuchs, M. Hrabe de Angelis, G. Schiavo, D. T. Shima, A. P. Russ, G. Stumm, J. E. Martin, E. M. Fisher, *Science* **2003**, 300, 808–812.
- [4] a) J. L. Ross, K. Wallace, H. Shuman, Y. E. Goldman, E. L. Holzbaur, *Nat. Cell Biol.* **2006**, 8, 562–570; b) R. J. McKenney, W. Huynh, M. E. Tanenbaum, G. Bhabha, R. D. Vale, *Science* **2014**, 345, 337–341.
- [5] B. Cui, C. Wu, L. Chen, A. Ramirez, E. L. Beare, W. P. Li, W. C. Mobley, S. Chu, *Proc. Natl. Acad. Sci. USA* **2007**, 104, 13666–13671.
- [6] a) F. Auzel, *Chem. Rev.* **2004**, 104, 139–174; b) F. Wang, S. Wen, H. He, B. Wang, Z. Zhou, O. Shimoni, D. Jin, *Light: Sci. Appl.* **2018**, 7, 18007; c) Q. Liu, Y. Zhang, C. Peng, T. Yang, J. Lydia-Marie, S. Chu, *Nat. Photonics* **2018**, 12, 548–553; d) K. Zheng, S. Han, X. Zeng, Y. Wu, S. Song, H. Zhang, X. Liu, *Adv. Mater.* **2018**, 30, 1801726; e) Y. Wang, K. Zheng, S. Song, D. Fan, H. Zhang, X. Liu, *Chem. Soc. Rev.* **2018**, 47, 6473–6485; f) L. Liang, X. Qin, K. Zheng, X. Liu, *Acc. Chem. Res.* **2019**, 52, 228–236; g) X. Qin, J. Xu, Y. Wu, X. Liu, *ACS Cent. Sci.* **2019**, 5, 29–42.
- [7] a) F. Wang, R. Deng, J. Wang, Q. Wang, Y. Han, H. Zhu, X. Chen, X. Liu, *Nat. Mater.* **2011**, 10, 968–973; b) L. Zhou, R. Wang, C. Yao, X. Li, C. Wang, X. Zhang, C. Xu, A. Zeng, D. Zhao, F. Zhang, *Nat. Commun.* **2015**, 6, 6938; c) R. Deng, F. Qin, R. Chen, W. Huang, M. Hong, X. Liu, *Nat. Nanotechnol.* **2015**, 10, 237–242; d) F. Wang, X. Liu, *Acc. Chem. Res.* **2014**, 47, 1378–1242.
- [8] a) S. Wu, G. Han, D. J. Milliron, S. Aloni, V. Altou, D. V. Talapin, B. E. Cohen, P. J. Schuck, *Proc. Natl. Acad. Sci. USA* **2009**, 106, 10917–10921; b) M. Yu, F. Li, Z. Chen, H. Hu, C. Zhan, H. Yang, C. Huang, *Anal. Chem.* **2009**, 81, 930–935; c) S. H. Nam, Y. M. Bae, Y. I. Park, J. H. Kim, H. M. Kim, J. S. Choi, K. T. Lee, T. Hyeon, Y. D. Suh, *Angew. Chem. Int. Ed.* **2011**, 50, 6093–6097; *Angew. Chem.* **2011**, 123, 6217–6221.
- [9] a) L. Xiong, Z. Chen, Q. Tian, T. Cao, C. Xu, F. Li, *Anal. Chem.* **2009**, 81, 8687–8694; b) S. Chen, A. A. Weitemier, X. Zeng, L. He, Y. Wang, Y. Tao, A. J. Y. Huang, Y. Hashimoto-dani, M. Kano, H. Iwasaki, L. K. Parajuli, S. Okabe, D. B. Loong Teh, A. H. All, I. Tsutsui-Kimura, K. F. Tanaka, X. Liu, T. J. McHugh,

- Science* **2018**, 359, 679–684; c) Y. Wang, X. Lin, X. Chen, X. Chen, Z. Xu, W. Zhang, Q. Liao, X. Duan, X. Wang, M. Liu, F. Wang, J. He, P. Shi, *Biomaterials* **2017**, 142, 136.
- [10] a) Y. Liu, Y. Lu, X. Yang, X. Zheng, S. Wen, F. Wang, X. Vidal, J. Zhao, D. Liu, Z. Zhou, C. Ma, J. Zhou, J. A. Piper, P. Xi, D. Jin, *Nature* **2017**, 543, 229–233; b) D. J. Gargas, E. M. Chan, A. D. Ostrowski, S. Aloni, M. V. P. Altoe, E. S. Barnard, B. Sanii, J. J. Urban, D. J. Milliron, B. E. Cohen, P. J. Schuck, *Nat. Nanotechnol.* **2014**, 9, 300–305; c) D. Jin, P. Xi, B. Wang, L. Zhang, J. Enderlein, A. M. van Oijen, *Nat. Methods* **2018**, 15, 415–423.
- [11] a) I. H. Yang, R. Siddique, S. Hosmane, N. Thakor, A. Höke, *Exp. Neurol.* **2009**, 218, 124–128; b) S. Hosmane, I. H. Yang, A. Ruffin, N. Thakor, A. Venkatesan, *Lab Chip* **2010**, 10, 741–747.
- [12] Y. Gu, W. Sun, G. Wang, K. Jeftinija, N. Fang, *Nat. Commun.* **2012**, 3, 1030.
- [13] A. J. Firestone, J. S. Weinger, M. Maldonado, K. Barlan, L. D. Langston, M. O'Donnell, V. I. Gelfand, T. M. Kapoor, J. K. Chen, *Nature* **2012**, 484, 125–129.
- [14] a) S. E. Encalada, L. Szpankowski, C. H. Xia, L. S. Goldstein, *Cell* **2011**, 144, 551–565; b) P. D. Chowdary, D. L. Che, L. Kaplan, O. Chen, K. Y. Pu, M. Bawendi, B. X. Cui, *Sci. Rep.* **2015**, 5, 18059.
- [15] a) J. C. Roux, D. Zala, N. Panayotis, A. Borges-Correia, F. Saudou, L. Villard, *Neurobiol. Dis.* **2012**, 45, 786–795; b) X. Xu, A. P. Kozikowski, L. Pozzo-Miller, *Front. Cell. Neurosci.* **2014**, 8, 68.
- [16] M. C. Marchetto, C. Carromeu, A. Acab, D. Yu, G. W. Yeo, Y. Mu, G. Chen, F. H. Gage, A. R. Muotri, *Cell* **2010**, 143, 527–539.
- [17] a) B. R. Schofield, *Current Protocols in Neuroscience*, Wiley, New York, **2008**, chap. 1, Unit 1 17; b) R. Apps, T. J. Ruigrok, *Nat. Protoc.* **2007**, 2, 1862–1868.
- [18] S. Ohara, S. Sato, K. Tsutsui, M. P. Witter, T. Iijima, *PLoS One* **2013**, 8, e78928.

Manuscript received: April 5, 2019

Revised manuscript received: April 26, 2019

Accepted manuscript online: May 14, 2019

Version of record online: May 28, 2019